On the Lessons Learned from the Operations of the ERBE Nonscanner Instrument in Space and the Production of the Nonscanner TOA Radiation Budget Dataset

Takmeng Wong[1*], G. Louis Smith[2,1], Seiji Kato[1], Norman G. Loeb[1], Greg Kopp[3], and Alok K. Shrestha[2]

[1]NASA Langley Research Center, Hampton VA

[2]Science Systems and Applications, Inc., Hampton VA

[3]University of Colorado/LASP, Boulder CO

***Corresponding author address: Takmeng Wong, MS 420, NASA Langley Research Center, Hampton, VA 23681 USA (email: takmeng.wong@nasa.gov)**

March 2018

Abstract

Monitoring the flow of radiative energy at top-of-atmosphere (TOA) is essential for understanding the Earth's climate and how it is changing with time. The determination of TOA global net radiation budget using broadband nonscanner instruments has received renewed interest recently due to advances in both instrument technology and the availability of small satellite platforms. The use of such instruments for monitoring Earth's radiation budget was attempted in the past from satellite missions such as the Nimbus 7 and the Earth Radiation Budget Experiment (ERBE). This paper discusses the important lessons learned from the operation of the ERBE nonscanner instrument and the production of the ERBE nonscanner TOA radiation budget data set that have direct relevance to current nonscanner instrument efforts.

I. Introduction

Earth's top-of-atmosphere (TOA) global net radiation budget involves a balance between how much solar energy Earth absorbs and how much terrestrial thermal infrared radiation is emitted to space. In an equilibrium climate, there is a global balance between these two quantities, albeit with considerable short-term and/or regional variability owing to internal variations within the climate system (e.g., weather, seasons, atmosphere-ocean interactions, etc.). When the climate system is forced by natural or anthropogenic factors, an imbalance in the TOA energy budget occurs that can lead to significant climatological changes as the system warms or cools in response to the forcing. Quantifying and monitoring changes in the Earth's energy imbalance (EEI) is thus critical to our understanding of the Earth's climate and its variability with time.

Hansen et al. [1] argue that assessment of EEI requires a target absolute measurement accuracy approaching 0.1 Wm^{-2}. Currently, there are two well established scientific methods of obtaining EEI [2] using either (1) in-situ ocean measurement through the global distribution of Argo profiling floats or (2) broadband satellite observations of the TOA radiation budget through measurements of both the total solar irradiance (TSI) and the global Earth total (longwave plus shortwave) outgoing radiation (TOR). Other observational methods of calculating EEI are also available. For example, EEI can be calculated from (1) the changes in global ocean heat content deduced indirectly from the residual of global ocean mass budget [3] using satellite data products from both the altimeter missions [4] and the Earth gravity mission [5] or (2) the changes in observed surface sensible, latent and radiative energy budget. These alternative methods, however, may contain large uncertainty [6]. In-situ ocean measurements from Argo network,

averaged over at least one decade, are highly accurate with absolute accuracy approaching 0.1 Wm^{-2} and can provide EEI near the desired climate accuracy requirement [7]. They are, however, much less useful at shorter timescales due to large sampling uncertainties. While satellite observations of the TOA radiation budget provide far better sampling than in-situ ocean measurements and are radiometrically stable to a few tenths of a Wm^{-2} per decade, they have yet to reach the target EEI absolute measurement accuracy of 0.1 Wm^{-2} [8].

Of the two components of the satellite-based TOA radiation budget observations, only the TSI satellite measurements currently have high enough absolute measurement-accuracy level (~0.03%) to pass the desired climate accuracy requirement [9], [10], [11]. Those direct solar measurements, being of a nearly-constant, bright, and nearly-collimated source with most of its energy in the visible and near-infrared, albeit being very difficult themselves, are much simpler than measuring the TOA TOR from the Earth. The latter requires measurements that cover (1) the entire broadband spectral range (i.e., full visible and near-, mid-, long-, and far-infrared radiation), (2) several-orders of magnitude dynamic range for spatially- and spectrally-varying scenes (i.e., dark oceans to bright clouds, day to night locations, bright continuum to dark spectral absorption lines, and the variations between bright visible and much lower near- and mid-infrared signals), and (3) the full angular sampling of the hemispherical Earth radiation field to account for non-isotropic scattering from various Earth scenes and their dependencies on solar and satellite viewing conditions. In addition to these measurement issues from a single TOA-monitoring instrument, many other factors further increase uncertainties in estimating the total outgoing TOA radiation, including (1) the need to cross-calibrate measurements

from the multiple sensors in orbits for complete diurnal sampling of global radiation fields and (2) adjustments for atmospheric losses and non-isotropic scattering that enables correction to a defined "TOA altitude". Thus, these satellite-based TOA TOR measurements include both intrinsic instrument uncertainties and other additional factors that currently limit the absolute accuracy of the global net radiation as needed for climate studies.

New technological advances have recently been proposed that purport to be able to reach an absolute accuracy of 0.3 Wm^{-2} or better from satellites for global Earth TOR [12]. The new technology involves using a small non-scanning sensor based upon a vertically aligned carbon nanotube (VACNT) absorber and Gallium blackbody emitter. A prototype instrument is being tested on the Radiometer Assessment using Vertically Aligned Nanotubes (RAVAN) mission [12]. RAVAN is a precursor to a more extensive mission concept involving many nonscanner instruments on multiple satellites (e.g., CubeSats). The use of broadband nonscanner instruments for measuring the global net radiation budget is not new, with such instruments aboard the Nimbus 7 satellite [13], [14] between 1978 and 1988 as well as on the Earth Radiation Budget Experiment (ERBE) mission [15] between 1985 and 2005. More recently, a European-lead PICARD satellite mission produced a limited 37-month data record of global net radiation from a nonscanner instrument [16]. Unfortunately, the on-orbit accuracies of these nonscanner instruments failed to meet their prelaunch accuracy goals owing to inherent challenges involved with calibrating these types of instruments both for and in the space environment. Importantly, the absolute accuracy goals for these early missions were of order 2 Wm^{-2}, roughly an order-of-magnitude less stringent compared to those promised for future missions flying

RAVAN-class nonscanner instruments [12]. How these new missions will overcome the on-orbit challenges experienced during the earlier nonscanner missions and meet such stringent absolute accuracy requirements remains unclear, as the new VACNT technology and the multiple-satellite approach do not alleviate all the difficulties mentioned above.

Given the current interest in nonscanner-type instrument missions for observing Earth's Radiation Budget (ERB), this paper reviews past working experience with these instruments by revisiting the important lessons learned from those that flew as part of the ERBE mission. Section II describes the ERBE mission and the nonscanner instrument that was used during that mission. Section III highlights the ERBE nonscanner data processing system from instrument-level data ingest to final scientific data product. Sections IV and V provide a discussion of outstanding issues encountered during ERBE and how these issues affected the absolute accuracy and the stability uncertainties of the scientific data product. Section VI provides a brief summary.

II. ERBE Mission

The ERBE mission was designed to capture the TOA ERB by flying broadband ERB instruments in a three-satellite configuration (ERBS, NOAA-9, and NOAA-10) in order to capture the full diurnal cycle of the Earth TOR fields [17]. The Earth Radiation Budget Satellite (ERBS) was placed in a precessing orbit with a 57° inclination and an altitude of 611 km. The ERBS orbit precessed through the entire 24-hour local time every 72 days. The National Oceanic and Atmospheric Administration - 9 (NOAA-9) and NOAA-10 satellites were in sun-synchronous orbits with 99º inclinations and altitudes of 860 km. The equatorial crossing times for the NOAA-9 and NOAA-10 satellites were 1430 LT

and 730 LT, respectively. While the NOAA-9 and NOAA-10 satellites provided global coverage, ERBS only viewed latitudes between 60° N and 60° S. Each ERBE satellite carried one scanner instrument package and one nonscanner instrument package.

A. ERBE Scanner Instrument

The ERBE scanner instrument, described by Kopia [18] and Halyo et al. [19], included a shortwave, a longwave, and a total channel radiometer. The scanner instrument scanned the Earth in a cross-track pattern to obtain maximum geographic coverage. The scanner footprint size was on the order of 30 – 40 km at nadir. This small scanner footprint allowed the determination of both clear-sky flux and all-sky flux, which can be used to define cloud radiative effects [20]. The scanner on ERBS operated from 11/1984 to 2/1990. The NOAA-9 scanner operated for 2 years from 2/1985 to 1/1987 and the NOAA-10 scanner operated for about 2.5 years from 11/1986 to 5/1989. The scanner data have been used extensively by the science community to understand the spatial and temporal distribution of the Earth radiation fields and the effect of clouds on the Earth radiation budget, and to provide a TOA radiative energy constraint to climate models [21], [22], [23].

B. ERBE Nonscanner Instrument

The ERBE nonscanner package was designed to measure radiative fluxes at a large spatial scale. This instrument viewed the Earth at its nadir pointing position during normal operation. Because of its mechanical simplicity, the nonscanners lasted much longer than the scanner instrument. For example, the nonscanner package on ERBS operated for 20 years from 11/1984 to 8/2005. The NOAA-9 nonscanner package

operated for 7 years from 2/1985 to 12/1992. The NOAA-10 nonscanner package operated for 8 years from 10/1986 to 11/1994. The ERBE nonscanner instrument, described in detail by Luther et al. [24] and Halyo et al. [19], was built using lessons learned from the previous satellite missions and represented the state-of-the-art ERB nonscanner instrument of the 1980's era. This instrument, shown in Fig. 1, was carefully designed and its components (mechanical, electronic, thermal, optical, and radiometric) were well characterized before launch [24], [19]. The nonscanner instrument package contained two wide-field-of-view (WFOV) and two medium-field-of-view (MFOV) channels for measuring both the total (0.2 to 50 μm) and the reflected shortwave radiation (0.2 to 5 μm). While the WFOV channels viewed the entire Earth disk from nadir to limb at the satellite's altitude, the MFOV channels had a footprint size of approximately 5º of Earth-central angle at the satellite altitude. Because of the large footprint size, the nonscanner instrument can only produce all-sky radiation products; there were no clear-sky data available from the nonscanner instrument.

The total and shortwave sensor technology on the nonscanner was based on the same type of active cavity radiometer (ACR) using blackbodies with a special, high-emittance, temperature-controlled design (stability within +/- 0.02 C). This high level of instrument thermal control was critical to the absolute accuracy of the ERBE nonscanner measurements. A hemispherical infrared-blocking fused-silica dome filter was placed in front of one set of WFOV and MFOV ACRs to acquire the shortwave-only measurements. The remaining set of ACRs without dome filters was used to measure the total radiation. The nonscanner channels were covered with an instrument cover plate before, during, and for a short period after launch to reduce contamination of the sensors

and dome filters. After the cover plate was removed, the instrument routinely performed both internal and solar calibrations by rotating the sensors 180º to view an on-board blackbody and tungsten lamp and by rotating the sensors 78º to view the Sun through the solar port (see Fig. 2), respectively. These measurements were used to determine instrument gains and zero-level offsets for correcting on-orbit calibration changes in instrument response throughout its mission. In addition, special satellite maneuvers were used to view the Sun as well as deep space directly to determine instrument gains and zero-level offsets at the beginning of and the end of the mission. These deep-space measurements also allowed corrections for background thermal effects from other components in the instrument package.

III. ERBE Nonscanner Data Processing System

Figure 3 shows a simple flow diagram of the ERBE nonscanner data processing system. It contained three major processing subsystems: instrument count conversion, TOA flux inversion, and time-space averaging. The most basic instrument level data was the instantaneous satellite altitude nonscanner voltage count. This voltage count was converted into scientific data (i.e., instantaneous satellite altitude nonscanner flux) using the ERBE nonscanner instrument count conversion algorithm. Uncertainty in instrument performance can directly affect the absolute accuracy of the count conversion process. The instantaneous satellite altitude flux was then converted into instantaneous TOA radiative flux using the ERBE nonscanner TOA flux inversion algorithm. Uncertainty in the ERBE inversion model can directly influence the absolute accuracy of the nonscanner TOA flux. Finally, the instantaneous TOA radiative fluxes were converted to a time (daily and monthly) and space (10-degree) averaged scientific data product using the

ERBE nonscanner time-space averaging algorithm. Non-uniform time and space sampling can be a source of uncertainty in this step. Fortunately, the ERBE time-space averaging uncertainty usually added noise to the final data product with minimum effect on overall absolute accuracy. The next two sections will discuss lessons learn from both nonscanner instrument operations and TOA data production.

IV. Lessons from Nonscanner Instrument Operations

While the radiometric performance of the WFOV nonscanner instrument was well documented and understood during pre-launch testing, the ERBE instrument team learned after launch that this type of instrument was inherently difficult to accurately calibrate on orbit due to issues encountered in the space environment. In the following, we highlight these calibration challenges using results from the ERBE WFOV instrument including:

- Removing the instrument radiometric drift, which impacted the stability of the radiative fluxes
- Accounting for changing instrument radiometric offsets, which affected the stability and absolute accuracy of the radiative fluxes
- Intercalibrating measurements from multiple on-orbit nonscanner instruments needed to provide full global diurnal coverage

A. On-orbit Instrument Gain Variations

The ERBE WFOV nonscanner was designed with a relative on-orbit calibration capability in order to determine instrument drifts with time. The radiometer viewed the

Sun and an internal calibration source every two weeks to monitor changes in instrument gains. Using this method, the on-orbit performance of the ERBS's total-channel ACR was determined to be stable to within 0.5 Wm^{-2} over 15-years [25]. The long-term performance of the shortwave channel was not quite as good. The root cause of the larger shortwave instrument degradation was determined to be decreasing optical transmission due to exposure of the WFOV shortwave dome to solar radiation during spacecraft sunrise, sunset, and bi-weekly solar calibration events. The magnitude of this degradation was time dependent and varied as a function of wavelength of shortwave radiation and the spatial pattern of the total cumulative solar dosage on the shortwave dome [26], [27]. Similar shortwave dome degradation issues also occurred with the Nimbus-7 nonscanner instrument [28]. These spectrally- and spatially-dependent effects were very difficult to account for once the instrument was in orbit. Fig. 4 shows the time series of the ERBS nonscanner WFOV total and shortwave instrument gain as a function of time, determined by the ERBS bi-weekly on-orbit solar calibration data [25]. The gain, which is equivalent to transmission throughput, was defined as unity at the beginning of the mission. Without the silica dome, the total sensor gain showed no sign of degradation with time. This was in contrast to the large change in gain for the shortwave sensor, which decreased 8.8% over the mission lifetime due to exposure to direct sunlight. Because of the lack of spectral and spatial information on the shortwave dome at the time of data processing, the ERBE instrument team assumed the dome degradation to be spectrally and spatially uniform. A simple time dependent shortwave gain correction was then developed based on these solar calibration data. This correction was applied to the original WFOV

nonscanner shortwave data by increasing the satellite shortwave measurement by a spectrally-independent ~8.8% over time.

While this simple solar-calibration correction was used successfully in fixing the majority of the shortwave dome problems, it did not completely eliminate all shortwave dome transmission related artifacts as seen in Fig. 5, which shows the time series of daytime and nighttime longwave flux over the tropics and the corresponding differences between them [29]. The nighttime longwave, deduced from the total channel alone, was stable over time. The daytime longwave, produced by subtracting the shortwave channel measurement from the total channel measurement, would normally be expected to show similar levels of stability, yet it showed an increase with time. The artificial growth of daytime longwave was consistent with a spectrally-dependent shortwave dome degradation effect in which the shorter wavelength signals (i.e., blue scene from clear ocean) degraded faster than their longer wavelength counterparts (i.e., cloudy scene). Such spectrally-dependent transmission degradation effects are typical of silica-based optics exposed to solar ultraviolet radiation. The spectrally flat ERBE nonscanner gain correction resulted in an artificially low shortwave signal and a correspondingly enhanced longwave signal, since the daytime longwave signal was calculated from the total minus the shortwave signals. The magnitude of this additional artifact on the shortwave flux was on the order of 1.5% over the 15-year period. This result suggested that solar calibration data alone cannot remove all shortwave instrument artifacts since the ERBE solar calibration correction assumed spectrally- and spatially- uniform dome degradation with time. In reality, the ERBE shortwave dome transmission loss was both spectrally and spatially dependent as noted earlier. It was nearly impossible to

discriminate and to completely remove these artifacts from the measurements after launch. The shortwave dome degradation, if left uncorrected, can alias into the long-term nonscanner data record. Wong et al. [29] developed a secondary correction for shortwave and longwave fluxes to remove these additional instrument artifacts using time series of tropical mean daytime minus nighttime longwave flux differences. This additional correction, while useful, did not completely remove spectral artifacts embedded in the regional data. The estimated uncertainty of this secondary correction was on the order of 0.1 Wm^{-2} for both shortwave flux and longwave flux at the end of the 15-year period. As a side note, it should be pointed out that shortwave spectral degradation issues are a universal satellite instrument problem affecting even the newer and more advanced scanner instruments such as those from the Clouds and the Earth's Radiant Energy System (CERES) mission [30] and the Geostationary Earth Radiation Budget (GERB) mission [31].

One solution to the shortwave dome degradation problem is to carry two sets of identical nonscanner shortwave instruments with the reference set completely shielded by a cover plate during Earth observations. This extra reference set is only opened for observations during solar calibration periods when the Earth-viewing instrument is also looking at the Sun at the same time. A shortwave gain correction can then be developed using measurements from both the Earth-viewing and reference sensors. This method can slow down the degradation artifact, but it does not completely remove it from the data since the reference shortwave instrument will also degrade during solar calibration periods. Another solution that may be possible in the future is to cross-calibrate the nonscanner shortwave measurement with other more accurate and stable sensors such as those from

the proposed National Aeronautics and Space Administration (NASA) Climate Absolute Radiance and Refractivity Observatory (CLARREO) mission [32] or the proposed National Physical Laboratory (NPL) Traceable Radiometry Underpinning Terrestrial- and Helio- Studies (TRUTHS) mission [33]. However, with a nonscanner instrument, this method also has challenges. Detailed discussion of this method is given in section IV-C.

B. On-orbit Instrument Offset Variations

Another on-orbit instrument issue that limited the stability and absolute accuracy achievable from ERBE nonscanners was the large uncertainty in instrument offset during the mission. The nonscanner flux was estimated using an engineering equation that consists of slopes and offsets to convert instrument count to a physical unit [19]. Thus an uncertainty in instrument offset value can directly affect the absolute accuracy of both the instantaneous and time-space averaged nonscanner flux data. On ERBE, the on-orbit nonscanner total channel offset was determined every 14 days based on internal blackbody measurements or blackbody energy calculated from internal temperature sensor measurements. The shortwave offset was derived using shortwave data collected during the nighttime orbit or from other internal calibration data during the bi-weekly calibration events. The non-zero shortwave value at night was used as the shortwave offset. Paden et al. [34] showed comparisons of offset values based on these different calibration methods. While the total channel offsets determined using the two calibration methods were in excellent agreement, the shortwave channel offsets differed by a few Wm^{-2} depending upon the calibration method used. This uncertainty therefore directly affected the absolute accuracy of the final nonscanner shortwave fluxes. Furthermore, shortwave offset uncertainty also affected the final nonscanner daytime longwave fluxes

since they were determined by subtracting the shortwave channel measurements from the total channel measurements.

In addition to the absolute uncertainty associated with the various calibration methods, there were also changes in zero-level offset on three different timescales during the ERBE mission: long-term drifts, short-term fluctuations, and instrument restart (power-cycling) level changes. These offset changes introduced additional uncertainties to the nonscanner dataset. Fig. 6 shows the time series of the ERBS WFOV nonscanner total and shortwave channel offsets from November 1984 to September 1999 [35]. While the total channel offset slowly drifted upward by about 12 Wm^{-2} over this 15-year period, the corresponding shortwave channel offset changed by approximately 100 Wm^{-2} over the same period. Ninety percent of the shortwave offset change can be accounted for by the shortwave dome degradation effect, leaving about 10 Wm^{-2} as the actual shortwave channel offset drift. Imbedded in the long-term drift were level shifts in offsets that were related to satellite anomaly events (i.e., battery or power issues). These satellite anomaly events resulted in the shutdown and consequent restart of the ERBS nonscanner instrument during the 15-year period. Each time this happened, the nonscanner offsets experienced a level shift of ~ 3 to 4 Wm^{-2}. These slow long-term offset drifts and instrument-restart offset level shifts, which affected the stability of the measurements, were caused by changes in electrical resistances of the wiring within the ERBE nonscanner [35], [36] and were corrected to ensure a high quality data product.

In addition to the long-term offset drifts and the instrument-restart level shifts, the ERBE nonscanner also experienced large short-term fluctuations in offsets that were attributed to changing thermal-background effects. These offsets fluctuation directly affected the

absolute accuracy of the measurements. Green et al [37] gave a detailed discussion of this issue based on comparisons between scanner and nonscanner measurements. For the total channel, they found that the nonscanner offset changed rapidly with time; it even varied significantly during one orbit. They showed the root cause of this short-term offset fluctuation can be traced to changes in solar illumination on the spacecraft and the associated varying thermal loads on the instrument. For example, they reported that the longwave measurement could change by more than 3% during spacecraft sunrise and sunset (Fig. 7). Longwave changes were also observed over the month as the ERBS orbit precessed from a terminator to a noon orbit. Again, they concluded that this was due to changes in instrument offsets associated with changing solar illumination on the spacecraft. They estimated that the absolute accuracy uncertainty of the nonscanner caused by the rapidly changing offset was on the order of 1 to 3 Wm^{-2} since such offset issues did not vanish in the time-space averaged dataset. The analysis also indicated that the offset changed depending on both the spacecraft position within the orbit and the satellite beta angle, which is a measure of solar exposure of the orbit. A beta angle of 0º indicates that the orbit is completely in the dark while a beta angle of 90º indicates that it is completely illuminated by the Sun. While the orbit dependence caused spurious latitudinal signals, the beta angle dependence caused longer term month to seasonal biases. These results strongly suggested that the short-term offset changes could have been caused by changes in temperature gradients inside the instrument even though the nonscanner had a built-in heater to maintain steady state temperature with time. The temperature gradient depended on solar heating, hence on orbit parameters. While the design global net absolute accuracy goal of the ERBE nonscanner was 1.7 Wm^{-2} [15], the

actual ERBE nonscanner in-flight global net absolute accuracy uncertainty was closer to 5 Wm^{-2} due to such instrument thermal-background uncertainties. This was, nevertheless, an improvement over the Nimbus 7 nonscanner, which had a global net absolute accuracy uncertainty of 10 Wm^{-2} [28], [38], [39].

This offset issue is not unique to satellite instruments. Offset issues caused by internal temperature gradients also exist for WFOV broadband flux instruments used for monitoring the surface radiation budget at ground level as part of the WMO Baseline Surface Radiation Network [40]. The magnitude of the offset fluctuation depends upon the instrument design as well as the environmental conditions in which the instrument is operated. The underlining physics causing the offset changes in ground and satellite sensors is similar. For example, the higher quality Kipp and Zonen shortwave (CP-22) and longwave (CGR-4) instruments have an uncertainty of 1 to 4 Wm^{-2} under much less extreme ground thermal environments than those of the deep-space viewing conditions ranging from 3 K to full solar heating on orbital timescales of ~90 minutes. Details of the Kipp and Zonen surface instrument accuracy specifications can be found at http://www.kippzonen.com/.

One limitation of the nonscanner is that the requirement to constantly view Earth leaves insufficient time to verify offsets continuously in space, but instead relies on intermittent internal blackbody calibration measurements or observations of deep space from special spacecraft maneuvers. This is in contrast to scanner operations, which see the Earth and deep space at each side of every temporally-short scan. The inability to determine instrument offsets continuously degrades the scientific usefulness of the WFOV

nonscanner data, resulting in a large uncertainty of 5 Wm^{-2} in the global net radiation at TOA and energy imbalance of planet Earth.

Thermal-background corrections affect all nonscanner instruments. The intrinsic instrument thermal background, even if stable, needs to be corrected for high-accuracy measurements. Improved thermal stability reduces the corrections and thus likely provides lower associated uncertainties. As a relatively large instrument, the ERBE benefitted from thermal mass; the smaller instruments desired for a CubeSat constellation to measure outgoing TOA radiation will likely not have this thermal-mass benefit.

One possible solution to the offset problem is to design new nonscanner ACRs to include an oscillating shutter, similar to those used in the Total Irradiance Monitor (TIM) instrument [41] on the Solar Radiation and Climate Experiment (SORCE) mission and to similarly acquire dark measurements using dark space to characterize the instrument's thermal background signals.

C. On-orbit Inter-Satellite Calibrations

In order to get accurate global net radiation, the diurnal cycle of radiation must also be captured. Since the outgoing TOA radiation is not isotropic, multiple look-angles of the same spatial regions are needed. The sampling requirement can be provided using a large fleet of WFOV nonscanner instruments in different orbits. However, intercalibrating nonscanner instruments on different satellites to a single radiometric standard is challenging. Since onboard solar and internal calibration sources have instrument intrinsic uncertainties due to the gain and offset drifts mentioned in the previous sub-sections, such drifts are unique to each nonscanner instrument, depending on its specific

space environment with time. In order to tie the nonscanner measurements on different platforms to a single standard, the instruments must be cross-calibrated. One approach might be to use the best performing nonscanner instrument as a reference and calibrate the others using overlapping footprints on Earth. For sun-synchronous satellites, the different satellite orbits intercept one another over the polar region. However, this region usually does not provide enough diversity of global sampling conditions to allow for accurate cross-calibration between individual nonscanner instruments. Specifically, the surface and atmospheric conditions over the polar region are very different from other climatological regions on Earth, so a cross-satellite calibration coefficient developed over the polar region may not apply to other climate regimes on Earth. Therefore, new methods of inter-satellite calibration must be developed to improve the accuracy of the combined satellite product.

One possible solution to improve future measurements is to inter-calibrate the WFOV nonscanner data with highly accurate and stable instruments from proposed satellite mission, such as the NASA CLARREO mission [32]. CLARREO is designed to be an absolute calibration observatory in space, and its measurement accuracy is directly traceable to international physical standards. The 2-sigma absolute-accuracy uncertainties of the CLARREO reflected solar and infrared instruments are less than 0.3% of Earth mean reflectance and 0.06 K, respectively. CLARREO will be placed in a 90º orbit at a satellite altitude of ~ 600 km for full diurnal sampling twice per year. During operation, the CLARREO satellite will intermittently acquire simultaneous measurements with other operational weather and climate satellites as it under-flies them. The observations from the highly accurate CLARREO instruments can be used to improve the accuracy of

these less accurate weather and climate instruments through such co-temporal and co-spatial cross-calibrations. Currently, there is no plan for the full CLARREO mission; only the CLARREO Pathfinder mission for reflected shortwave measurements on the International Space Station (ISS) is planned, with a launch in the 2020 time-frame as a technology demonstration [42].

While the CLARREO concept is very useful for many weather and climate instruments, it cannot be used directly to improve the accuracy of the WFOV nonscanner instrument due to the mismatch of the instrument footprint size and the length of the satellite swath. The current design of the CLARREO infrared instrument is a nadir-viewing sensor with the footprint size of about 100 km. The reflected solar instrument has a footprint size of 0.5 km and a satellite swath width of 100 km. These are in contrast to the WFOV nonscanner footprint size of 1000 km. These spatial mismatches mean that the CLARREO measurements can never completely spatially fill the larger WFOV nonscanner footprint, which is required for accurate cross-calibration analysis relying on simultaneous measurements.

Alternately, the nonscanner can be indirectly tied to CLARREO by flying in formation with other cross-track broadband scanner instruments such as CERES. These scanners can be used as the link between a nonscanner and CLARREO by first tying the scanner directly to the CLARREO measurements through overlap measurements, and then tying the nonscanner to the calibrated scanner measurements by integrating the scanner data over the nonscanner footprint using the technique of Green et al. [37]. It should be noted that angular distribution models (ADMs) are needed in order to correctly account for CERES viewing geometry within the larger nonscanner field-of-view. The uncertainty of

this procedure is on the order of 1% for shortwave flux and 0.5% for longwave flux [43]. Once this nonscanner instrument is indirectly tied to CLARREO, it can be used to cross-calibrate other nonscanner satellites in a possible constellation. Each such inter-calibration will, of course, successively increase uncertainties. Due to the large footprint of the WFOV nonscanner instrument, a multi-satellite mission must be carefully designed in order to provide maximum overlap between instruments over a large dynamic range of surface and atmospheric conditions all over the globe in a way to maximize inter-satellite calibration data collection.

Uncertainties due to inter-calibrations affect both the relative accuracies of relating individual instruments to the mean of an entire constellation of which they may be a part and to on-orbit inter-calibration to another on-orbit standard, such as proposed CLARREO mission. While there were very few nonscanners in the three ERBE spacecrafts, these inter-calibration issues will need to be addressed for constellations having numerous separate instruments.

V. Lessons from Nonscanner TOA Data Production

In addition to instrument calibration concerns, the ERBE WFOV nonscanner data product also encountered other technical issues related to the construction of the TOA dataset from satellite measurements. These non-instrument related issues, which also affected the stability and absolute accuracy of the final WFOV nonscanner TOA dataset, include:

- Converting the instrument radiometric measurements to radiative fluxes at a single, defined TOA “altitude”, which affected the absolute accuracy of the TOA radiative fluxes

- Removing time-dependent artifacts of changes in satellite altitude, which impacted the stability of the TOA radiative fluxes
- Highlighting the effects from partial illumination of the sunlit and dark portions within a footprint when viewing the day-night terminator, which can potentially create a sampling bias to the TOA radiative fluxes

A. TOA Flux Inversion

Nonscanner measurements are taken from satellites that orbit Earth at an altitude of several hundred kilometers above sea level. In order to use these data for climate studies, the satellite altitude measurement must be converted to flux at a TOA reference altitude, which is the altitude where the observed flux can be compared with the flux computed with a plane parallel assumption. For the ERBE mission, this altitude was defined to be 30 km above sea level [44]. The CERES mission further refined this TOA reference altitude value to be 20 km [45]. Since this TOA altitude is usually much lower than the satellite altitude, where the actual measurements are made, a flux inversion method has been developed over the years to convert these satellite measurements into TOA fluxes. The conversion factor depends on the angular distribution of radiances. The flux inversion method, therefore, works best if the total (shortwave plus longwave) outgoing radiation is separated into its shortwave and longwave components because the angular distribution of the two differ; furthermore, spectrally-dependent differences on finer scales are also expected within each bandpass. In addition, the longwave radiation is not sensitive to the position of the Sun and its inversion to TOA flux can be done using a simple formulation. The shortwave radiation, on the other hand, requires a more advanced method to convert the measurements into TOA fluxes due to its dependence on

solar viewing conditions. There are two common methods for inverting nonscanner satellite measurements to TOA fluxes: the shape factor method [46], [47], [48], [49] and the deconvolution method [50], [51]. While the shape factor method can convert any single nonscanner measurement into TOA flux without requiring neighboring nonscanner data, the deconvolution method requires contiguous and complete global nonscanner measurements to produce a single TOA flux [52]. Each of these two methods contains their own specific set of assumptions that can affect the accuracy of the inverted TOA fluxes [52]. The derivation of the shortwave shape factor, which was used to convert ERBE satellite measurements into TOA fluxes, contained assumptions about both the viewed radiation fields (i.e., mostly cloudy ocean) and the angular distribution of the radiance. Green and Smith [44] examined how these assumptions can affect the accuracy of the inverted instantaneous nonscanner MFOV and WFOV nonscanner TOA fluxes. Their results indicated that the TOA flux bias error for the shortwave shape factor inversion method were the worst for cases using the Lambertian radiation field assumption, with uncertainties ranging from 2% (~ -4 Wm^{-2}) for WFOV to 11% (~ -22 Wm^{-2}) for MFOV. The inversion regional RMS (i.e., bias plus random) error for this case was very large for both WFOV (~10%) and MFOV (~15%) TOA flux. Under more realistic conditions using ERBE ADMs for anisotropy of shortwave radiation [53], [54], the inversion TOA flux bias errors became more reasonable with values less than 1 Wm^{-2}. The inversion regional RMS errors, however, remained quite large with values ranging from 7% for WFOV to 10% for MFOV TOA flux. These results indicate the current accuracy limits of the ERBE nonscanner TOA flux inversion process, and are largely independent of intrinsic instrument accuracy.

B. Effect of Satellite Altitude Changes

Changes in satellite altitude can affect the long term quality of the nonscanner TOA flux value through the TOA flux inversion process because the WFOV shape factor inversion is proportional to the inverse-square of the distance between the satellite and the center of the Earth. Consequently, the inverted shortwave and longwave TOA fluxes from a descending satellite can slowly increase with time if the satellite altitude is not taken into account. This artifact, if not corrected for, can alias into the long term record of the nonscanner TOA radiation data set. Fig. 8 shows the changes in ERBS altitude over the 15-year period between 1985 and 1999 and the effect of this change on the long term ERBS nonscanner WFOV TOA radiation record. As the ERBS altitude slowly decreased from 611 km to 585 km over the 15-year period, the computed nonscanner WFOV longwave and shortwave TOA flux increased by 0.7%. This translated into an increase of ~1.5 Wm^{-2} for TOA outgoing longwave flux and an increase of ~0.7 Wm^{-2} for TOA reflected shortwave flux over the 15-year period. This satellite altitude effect was not corrected in the original ERBS WFOV nonscanner data set and had contributed to the reported large decadal changes in tropical mean TOA radiation budget between the 1980's and the 1990's [55]. When this satellite altitude artifact was finally corrected in the updated version of the ERBS WFOV nonscanner data set [29], the revised data showed a smaller decadal change in the tropical mean TOA radiation budget. The final updated ERBS WFOV nonscanner radiation budget record, which also included the additional shortwave dome degradation correction, was thereafter also more consistent with two other satellite radiation budget data sets.

The effect of satellite altitude changes is a simple but demonstrably needed correction that must be applied. This is especially important for a CubeSat constellation which may have limited satellite altitude maneuver capability. The spacecraft altitude itself is very well known, so this correction, when applied, has negligibly small uncertainties.

C. Partially-Illuminated Nonscanner Footprints

As the satellite crosses the day-night terminator region, the satellite measurement record includes footprints partially illuminated by the Sun. While these footprints have negligible impact on the quality of the TOA flux record for instruments with small footprint sizes (i.e., scanner instruments), the impact is far greater for nonscanner instruments since the fraction of footprints affected by the terminator is large owing to the large nonscanner footprint size (~1000 km). The ERBS WFOV nonscanner contained partially-illuminated footprints at a solar zenith angle between 90° and 118°. The inversion of these satellite footprint measurements into TOA fluxes can be problematic. The ERBE shortwave data beyond a solar zenith angle of 90° were usually discarded during nonscanner data processing. It is not completely clear how these discarded data can affect the overall accuracy of the nonscanner radiation data record, but it is known that the reflected shortwave flux can be detected from space for local solar zenith angles up to 105° [56]. For the CERES mission, Kato and Loeb [56] estimated that the missing CERES scanner twilight flux, defined as shortwave flux beyond solar zenith angle of 90°, was on the order of 0.2 Wm^{-2} for global mean and up to 1 Wm^{-2} over the polar regions. Thus the discarded nonscanner data will certainly create a bias of at least 0.2 Wm^{-2} in the global mean nonscanner shortwave flux. The actual bias value is probably much higher due to the larger nonscanner footprint size. Furthermore, this bias does not decrease even

for a multi-satellite mission since these partially-illuminated regions are usually locked into specific local time and they can only be observed by sun-synchronous satellite flying on a terminator orbit. Multi-satellite mission data from other non-terminator sun-synchronous satellites will not encounter these partially-illuminated regions.

Measurements with better spatial resolution or more sophisticated modeling of scatter near the terminator may improve these uncertainties, but they will nevertheless affect all nonscanners due to those instruments' large footprints.

VI. Summary

Continuous monitoring of the global net radiation budget at top-of-atmosphere (TOA) is critical to our understanding of the Earth's climate and its variability with time. The determination of TOA global net radiation budget using broadband nonscanner instruments has received renewed interest lately. This paper summarizes the important lessons learned from both the operation of the ERBE nonscanner instrument in space and the production of the ERBE nonscanner TOA flux data set.

While the ERBE nonscanner instruments were well characterized before launch, the ERBE team encountered significant issues related to post-launch instrument calibration. While the full spectral range "total" channel performed well in space with a radiometric stability approaching 0.5 Wm^{-2} over a 15-year period, the radiometric stability of the shortwave channel, which contained a silica dome filter, was problematic with gain (or transmission throughput) decreasing by 8.8% over the same period. The root cause for the poor performance of the shortwave channel was due to the large optical degradation of the dome due to exposure to direct sunlight over time. Since the nature of this

degradation was both spectrally and spatially dependent, the correction of these data was challenging. Using a simple spectrally and spatially uniform degradation assumption did not completely remove all shortwave instrument artifacts in the TOA dataset, as illustrated by the ERBE daytime minus nighttime longwave fluxes.

In addition to gain stability concerns, achieving stability and absolute accuracy requirements with ERBE nonscanner instruments wers exceedingly challenging due to large variations in instrument offsets in space. Besides the offset uncertainty that occurred from the calibration methods, there were also changes in zero-level offsets on three different timescales during the ERBE mission: long-term drift, short-term fluctuation, and instrument-restart level changes. The long-term drift and instrument-restart level changes, which affected the stability of the measurements, were likely caused by changes in electrical resistances of the wiring within the nonscanner. While the long-term offset drifts and the instrument-restart level shift were correctable, the nonscanner also experienced large short-term fluctuations in offsets that were attributed to changing thermal-background effects. The root cause can be traced to changes in solar illumination conditions on the spacecraft and the associated varying thermal loads on the instrument, which caused time-dependent temperature gradients within the instrument. While the designed global net absolute accuracy of the ERBE nonscanner measured in the laboratory was on the order of 1.7 Wm^{-2}, the actual in-flight ERBE nonscanner global net absolute accuracy uncertainty was closer to 5 Wm^{-2} due to instrument offset uncertainty.

The intercalibration of the nonscanner instruments on sun-synchronous satellites was also problematic. This is a general problem for instruments in sun-synchronous orbits because overlapping footprints needed to generate cross-satellite corrections can only be found in

the polar region, which has very different radiative energy signatures than the rest of the globe. Even direct cross calibrations with highly accurate instruments such as those proposed for CLARREO-like mission are difficult due to mismatched footprint sizes. However, it may be possible to indirectly tie a nonscanner to CLARREO-like instrument through cross-calibration by using a close-formation satellite mission that pairs a CERES instrument with a cloud imager. Such an indirect calibration method still contains uncertainties (averages of 1% in shortwave and 0.5% in longwave) associated with the usage of ADMs, and additional studies would be required to validate this concept.

Radiation budget measurements at satellite altitude must be converted to TOA flux before they can be used for climate studies. This inversion process generates large uncertainties for TOA flux, especially for shortwave data, due to the strong dependence on solar viewing conditions. While shortwave shape factor inversion using realistic ERBE ADMs for anisotropy of shortwave radiation can generate reasonable TOA flux, with inversion TOA bias errors of less than 1 Wm^{-2}, the inversion RMS errors (i.e., bias plus random error) can range between 7% for WFOV and 10% for MFOV TOA flux. A new nonscanner shortwave shape factor constructed using new CERES data may help further reduce the inversion errors. In addition, because of their large footprint size, nonscanner twilight measurements from footprints partially illuminated by the Sun cannot be ignored and need to be converted from satellite altitude to TOA flux. The conversion of fluxes for such footprints adds extra challenges in producing TOA global flux data particularly from the shortwave WFOV instrument.

Changes in satellite altitude can affect the TOA flux through the TOA flux inversion process, which can alias into the long-term record of the nonscanner data record. The

ERBS satellite altitude change affected the long term nonscanner record by increasing TOA outgoing longwave flux by 1.5 Wm^{-2} and TOA reflected shortwave flux by 0.7 Wm^{-2} over the 15-year period before corrections were applied in 2006.

Table I summarizes the global annual mean uncertainties of the ERBE nonscanner TOA fluxes after applying the specific corrections discussed in this paper. While the ERBE nonscanner data showed excellent long term stability after corrections, the absolute accuracy of this dataset remains problematic. The largest source of the absolute accuracy uncertainty for the nonscanner TOA data is from instrument offset determination (±2.5 Wm^{-2} for longwave and ±2.5 Wm^{-2} for shortwave). This is followed by intercalibration uncertainty between satellites and TOA flux inversion uncertainty, which range from ±1.0 to ±1.2 Wm^{-2}. Even with improvements in instrument measurement accuracy (i.e., no intrinsic instrument errors), the global mean nonscanner TOA flux is still limited by the accuracy of the current TOA flux inversion method, which is only accurate to within ±1 Wm^{-2}. Given the challenges discussed in this paper and the remaining data uncertainties shown in Table I, a complete end-to-end (i.e., from instrument to final data product) rework of the nonscanner concept is needed to meet the stringent requirements of attaining an absolute accuracy goal of 0.1 Wm^{-2} TOA flux for climate science. Specifically, the basic design of the nonscanner ACR must be improved in order to meet the high accuracy goals needed to study and track the global net energy with time. The current nonscanner instrument offset problems due to varying thermal conditions in space must be corrected with new instrument design in order to improve the overall accuracy of the nonscanner measurement. An improved TOA inversion algorithm and a better inter-satellite calibration method are also needed to improve the accuracy of the future

nonscanner data product. Finding solutions to these outstanding ERBE issues will greatly benefit future nonscanner missions.

Acknowledgements

This work is supported by NASA Science Mission Directorate through both the NASA CERES project and the NASA MEaSUREs project.

References:

[1] J. Hansen, M. Sato, P. Kharecha, and K. von Schuckmann, "Earth's energy imbalance and implications," *Atmos. Chem. Phys*., vol. 11, pp. 13421–13449, 2011, DOI:10.5194/acp-11-13421-2011.

[2] M. D. Palmer, "Reconciling Estimates of Ocean Heating and Earth's Radiation Budget," *Curr. Clm. Change Rep.*, vol. 3(1), pp. 78-86, 2017, DOI:10.1007/s40641-016-0053-7.

[3] S. R. Jayne and J. M. Wahr, "Observing ocean heat content using satellite gravity and altimetry," *J. Geophys. Res*., vol. 108, no. C2, 3031, 2003, DOI:10.1029/2002JC001619.

[4] R. S. Nerem, D. P. Chambers, C. Choe, and G. T. Mitchum, "Estimating Mean Sea Level Change from the TOPEX and Jason Altimeter Missions," *Marine Geodesy*, vol. 33, 435-446, 2010, DOI: 10.1080/01490419.2010.491031.

[5] J. L. Chen, C. R. Wilson, and B. D. Tapley, "Contribution of ice sheet and mountain glacier melt to recent sea level rise," *Nature Geosci*., vol. 6, 549-552, 2013, DOI: 10.1038/NGEO1829.

[6] K. Von Schuckmann, M. D. Palmer, K. E. Trenberth, A. Cazenave, D. Chambers, N. Champollion, J. Hansen, S. A. Josey, N. Loeb, P.-P. Mathieu, B. Meyssignac, and M. Wild, " An imperative to monitor Earth's energy imbalance," *Nature Clim. Change*, vol. 6, 138-144, 2016, DOI: 10.1038/NCLIMATE2876.

[7] G. C. Johnson, J. M. Lyman, and N. G. Loeb, "Improving estimates of Earth's energy imbalance," *Nature Climate Change*, vol. 6, pp. 639-640, 2016, DOI:10.1038/nclimate3043.

[8] N. G. Loeb, B. A. Wielicki, D. R. Doelling, G. L. Smith, D. F. Keyes, S. Kato, N. Manalo-Smith, and T. Wong, "Toward Optimal Closure of the Earth's Top-of-Atmosphere Radiation Budget," *J. Climate*, vol. 22, pp. 748–766, 2009, DOI:10.1175/2008JCLI2637.1.

[9] G. Kopp, G. Lawrence, and G. Rottman, "The Total Irradiance Monitor (TIM): Science Results," *Solar Physics*, vol. 230, no. 1, pp. 129-140, Aug. 2005, DOI:10.1007/s11207-005-7433-9.

[10] G. Kopp and J. L. Lean, "A New, Lower Value of Total Solar Irradiance: Evidence and Climate Significance," *Geophys. Res. Letters*, vol. 38, L01706, 2011, DOI:10.1029/2010GL045777.

[11] W. Schmutz, A. Fehlmann, W. Finsterle, G. Kopp, and G. Thuillier, "Total Solar Irradiance Measurements with PREMOS/PICARD," *AIP Conf. Proc*., vol. 1531, pp. 624-627, 2013, DOI:10.1063/1.4804847.

[12] W. H. Swartz, L. P. Dyrud, W. J. Wiscombe, S. R. Lorentz, S. J. Papadakis, D. L. Wu, R. A. Summers, and V. E. Wells, "Measuring Earth's radiation imbalance with RAVAN: A CubeSat mission to measure the driver of global climate change," *Earthzine*, December 2013. Accessed on July 12, 2016, [Online]. Available: http://www.earthzine.org/2013/12/02/measuring-earths-radiation-imbalance-with-ravan-a-cubesat-mission-to-measure-the-driver-of-global-climate-change/.

[13] H. Jacobowitz and R. J. Tighe, "The Earth Radiation Budget derived from the NIMBUS 7 ERB Experiment," *J. Geophys. Res*., vol. 89, no. D4, pp. 4997–5010, 1984, DOI:10.1029/JD089iD04p04997.

[14] H. L. Kyle, E. J. Hurley, and P. Ardanuy, "The Status of the Nimbus-7 Earth-Radiation-Budget Data Set," *Bull. Amer. Meteor. Soc*., vol. 66, pp. 1378–1388, 1985, DOI:10.1175/1520-0477(1985)066<1378:TSOTER>2.0.CO;2.

[15] B. R. Barkstrom, "The Earth Radiation Budget Experiment (ERBE)," *Bull. Amer. Meteor. Soc.*, vol. 65, pp. 1170–1185, 1984, DOI:10.1175/1520-0477(1984)065<1170:TERBE>2.0.CO;2.

[16] P. Zhu, M. Wild, M. van Ruymbeke, G. Thuillier, M. Meftah, and O. Karatekin, "Interannual variation of global net radiation flux as measured from space," *J. Geophys. Res. Atmos.*, vol. 121, pp. 6877–6891, 2016, DOI:10.1002/2015JD024112.

[17] E. F. Harrison, P. Minnis, and G. Gibson, "Orbital and cloud cover sampling analyses for multisatellite earth radiation budget experiments," *Journal of Spacecraft and Rockets*, vol. 20, no. 5, pp. 491-495, 1983, DOI:10.2514/3.25634.

[18] L. P. Kopia, "Earth Radiation Budget Experiment Scanner Instrument," *Rev. Geophys*., vol. 24, no. 2, pp. 400–406, 1986, DOI:10.1029/RG024i002p00400.

[19] N. Halyo, D. K. Pandey, and D. B. Taylor, "Modeling and Characterization of the Earth Radiation Budget Experiment (ERBE) Nonscanner and Scanner Sensors," *NASA Contractor Report NASA-CR-181818*, 1989. [Online]. Available: https://hdl.handle.net/2060/19890015401.

[20] V. Ramanathan, R. D. Cess, E. F. Harrison, P. Minnis, B. R. Barkstrom, E. Ahmad, D. Hartmann, "Cloud-Radiative Forcing and Climate: Results from the Earth Radiation Budget Experiment. Science," vol. 243, no. 4887, pp. 57-63, 1989, DOI:10.1126/science.243.4887.57.

[21] J. T. Kiehl, J. J. Hack, and B. P. Briegleb, "The simulated Earth radiation budget of the National Center for Atmospheric Research community climate model CCM2 and

comparisons with the Earth Radiation Budget Experiment (ERBE)," *J. Geophys. Res*., vol. 99, no. 10, 20815-20827, 1994, DOI: 10.1029/94JD00941.

[22] F. A.-M. Bender, "A note on the effect of GCM tuning on climate sensitivity," *Environ. Res. Lett*., vol 3, no. 1, 014001, 2008, DOI: 10.1088/1748-9326/3/1/014001.

[23] M. Huber, I. Mahlstein, M. Wild, J. Fasullo, and R. Knutti, "Constraints on climate sensitivity from radiation patterns in climate models," *J. Clim*., vol. 24, 1034-1052, 2011, DOI: 10.1175/2010JCLI3403.1.

[24] M. R., Luther, J. E. Cooper, and G. R. Taylor, "The Earth Radiation Budget Experiment Nonscanner Instrument," *Rev. Geophys*., vol. 24, no. 2, pp. 391–399, 1986, DOI:10.1029/RG024i002p00391.

[25] R. B. Lee, R. S. Wilson, G. L. Smith, K. A. Bush, S. Thomas, D. K. Pandey, J. Paden, "On-orbit characterizations of Earth Radiation Budget Experiment broadband shortwave active cavity radiometer sensor responses," *Proc. SPIE 5660, Instruments, Science, and Methods for Geospace and Planetary Remote Sensing*, pp. 23-35, 2004, DOI:10.1117/12.578822.

[26] G. L. Smith, R. B. Lee, and J. Paden, "Dome Degradation Pattern of the ERBE Wide Field-of-View Shortwave Radiometer," *Proc. SPIE, 4881, Sensors, Systems, and Next-Generation Satellites VI*, pp. 369-377, 2003, DOI:10.1117/12.462516.

[27] G. L. Smith, R. B. Lee, III, T. Wong, and P. E. Mlynczak, "Degradation pattern of the ERBE wide field-of-view radiometer aboard the NOAA 9 spacecraft," *Proc. SPIE 7106, Sensors, Systems, and Next-Generation Satellites XII*, pp. 71060X1-71060X9, 2008, DOI:10.1117/12.799637.

[28] H. L. Kyle, R. Hucek, P. Ardanuy, L. Penn, J. Hickey, and B. Groveman, "In-Flight Calibration of the Nimbus-7 Earth Radiation Budget (ERB) Sensors. Part I: A Thermal Model for the Shortwave Channels," *J. Atmos. Oceanic Technol*., vol. 12, pp. 1137–1149, 1995, DOI:10.1175/1520-0426(1995)012<1137:IFCOTE>2.0.CO;2.

[29] T. Wong, B. A. Wielicki, R. B. Lee, III, G. L. Smith, K. A. Bush, and J. K. Willis, "Re-examination of the Observed Decadal Variability of Earth Radiation Budget using Altitude-corrected ERBE/ERBS Nonscanner WFOV data," *J. Climate*, vol. 19, pp. 4028-4040, 2006, DOI:10.1175/JCLI3838.1.

[30] G. Matthews, "In-flight spectral characterization and calibration stability estimates for the Clouds and the Earth's Radiant Energy System (CERES)," *J. Atmos. Ocean. Tech*., vol. 26, 1685-1716, 2009, DOI: 10.1175/2009JTECHA1243.1.

[31] R. Parfitt, J. E. Russell, R. Bantges, N. Clerbaux, H. Brindley, "A study of the time evolution of GERB shortwave calibration by comparison with CERES Edition-3A

data," *Remote Sens. Environ.*, vol. 186, 416-427, 2016, DOI: 10.1016/J.RSE.2016.09.005.

[32] B. A. Wielicki, D. F. Young, M. G. Mlynczak, K. J. Thome, S. Leroy, J. Corliss, J. G. Anderson, C. O. Ao, R. Bantges, F. Best, K. Bowman, H. Brindley, J. J. Butler, W. Collins, J. A. Dykema, D. R. Doelling, D. R. Feldman, N. Fox, X. Huang, R. Holz, Y. Huang, Z. Jin, D. Jennings, D. G. Johnson, K. Jucks, S. Kato, D. B. Kirk-Davidoff, R. Knuteson, G. Kopp, D. P. Kratz, X. Liu, C. Lukashin, A. J. Mannucci, N. Phojanamongkolkij, P. Pilewskie, V. Ramaswamy, H. Revercomb, J. Rice, Y. Roberts, C. M. Roithmayr, F. Rose, S. Sandford, E. L. Shirley, W. L. Smith Sr., B. Soden, P. W. Speth, W. Sun, P. C. Taylor, D. Tobin, and X. Xiong, "Achieving Climate Change Absolute Accuracy in Orbit," *Bull. Amer. Meteor. Soc.*, vol. 94, pp. 1519–1539, 2013, DOI:10.1175/BAMS-D-12-00149.1.

[33] P. D. Green, N. P. Fox, D. Lobb, J. Friend, "The Traceable Radiometry Underpinning Terrestrial and Helio Studies (TRUTHS) mission," *Proc. SPIE 9639, Sensors, Systems, and Next-Generation Satellites XIX*, vol. 9639, 96391C, 2015, DOI: 10.1117/12.2192593.

[34] J. Paden, D. K. Pandey, R. Wilson, S. Thomas, M. A. Gibson, and R. B. Lee III, "Ground and in-flight calibrations for the earth radiation budget experiment (ERBE) nonscanning radiometers," *Proc. SPIE, 1300, Remote Sensing of the Biosphere*, pp. 190-201, 1990, DOI:10.1117/12.21407.

[35] R. L. Lee, III, J. Paden, D. K. Pandey, R. S. Wilson, K. A. Bush, and G. L. Smith, "On-orbit radiometric calibrations of the earth Radiation Budget Experiment (ERBE) active-cavity radiometers on the Earth Radiation Budget Satellite (ERBS)," *Proc. SPIE 4814*, pp. 369-379, 2002, DOI:10.1117/12.451614.

[36] B. A. Wielicki, A. D. Del Genio, T. Wong, J. Chen, B. E. Carlson, R. P. Allan, F. Robertson, H. Jacobowitz, A. Slingo, D. Randall, J. T. Kiehl, B. J. Soden, C. T. Gordon, A. J. Miller, S.-K. Yang, and J. Susskind, "Technical Response: Changes in Tropical Clouds and Radiation," *Science*, vol. 296, no. 2095a, 2002, DOI:10.1126/science.296.5576.2095a.

[37] R. N. Green, F. B. House, P. W. Stackhouse, X. Wu, S. A. Ackerman, W. L. Smith, and M. J. Johnson, "Intercomparison of scanner and nonscanner measurements for the Earth Radiation Budget Experiment," *J. Geophys. Res.*, vol 95, no. D8, pp. 11785–11798, 1990, DOI:10.1029/JD095iD08p11785.

[38] H. L. Kyle, R. Hucek, P. Ardanuy, L. Penn, B. Groveman, J. Hickey, and R. Maschoff, "In-Flight Calibration of the Nimbus-7 Earth Radiation Budget (ERB) Sensors. Part II: Short-Term Perturbations," *J. Atmos. Oceanic Technol.*, vol. 12, pp. 1150–1162, 1995, DOI:10.1175/1520-0426(1995)012<1150:IFCOTE>2.0.CO;2.

[39] H. L. Kyle, R. Hucek, P. Ardanuy, L. Penn, and B. Groveman, "In-Flight Calibration of the Nimbus-7 Earth Radiation Budget (ERB) Sensors. Part III: Long-Term Changes," *J. Atmos. Oceanic Technol*., vol. 12, pp. 1163–1176, 1995, DOI:10.1175/1520-0426(1995)012<1163:IFCOTE>2.0.CO;2.

[40] M. Haeffelin, S. Kato, A. M. Smith, C. K. Rutledge, T. P. Charlock, and J. R. Mahan, "Determination of the thermal offset of the Epply precision spectral pyranometer," *Appl. Opt*., vol. 40, pp. 472-484, 2001, DOI:10.1364/AO.40.000472.

[41] G. Kopp and G. Lawrence, "The Total Irradiance Monitor (TIM): Instrument Design," *Solar Physics*, vol. 230, no. 1, pp. 91-109, Aug. 2005, DOI:10.1007/s11207-005-7446-4.

[42] N. G. Loeb, W. Su, and S. Kato, "Understanding Climate Feedbacks and Sensitivity using Observations of Earth's Energy Budget," *Curr. Clim. Change Rep*., vol. 2, no. 4., pp. 170-178, 2016, DOI:10.1007/s40641-016-0047-5.

[43] A. K. Shrestha, S. Kato, T. Wong, D. A. Rutan, W. F. Miller, F. G. Rose, G. L. Smith, K. M. Bedka, P. Minnis, and J. R. Fernandez, "Unfiltering Earth Radiation Budget Experiment (ERBE) scanner radiances using the CERES algorithm and its evaluation with nonscanner observations," *J. Atmos. Ocean. Tech.*, 31, no. 4, pp. 843-859, 2014, DOI:10.1175/JTECH-D-13-00072.1.

[44] R. N. Green and G. L. Smith, "Shortwave Shape Factor Inversion of Earth Radiation Budget Observations," *J. Atmos. Sci*., vol. 48, pp. 390–402, 1991, DOI:10.1175/1520-0469(1991)048<0390:SSFIOE>2.0.CO;2.

[45] N. G. Loeb, S. Kato, and B. A. Wielicki, "Defining Top-of-the-Atmosphere Flux Reference Level for Earth Radiation Budget Studies," *J. Climate,* vol. 15, pp. 3301–3309, 2002, DOI:10.1175/1520-0442(2002)015<3301:DTOTAF>2.0.CO;2.

[46] W. L. Smith, J. Hickey, H. B. Howell, H. Jacobowitz, D. T. Hilleary and A. J. Drummond, "Nimbus 6 Earth Radiation Budget Experiment," *Appl. Opt*., vol. 16, pp. 306-318, 1977, DOI:10.1364/AO.16.000306.

[47] H. Jacobowitz, W. L. Smith, H. B. Howell, F. W. Nagle and J. R. Hickey, "The first 18 months of planetary radiation budget measurements from the Nimbus 6 ERB experiment," *J. Atmos. Sci*., vol. 36, pp. 501-507, 1979, DOI:10.1175/1520-0469(1979)036<0501:TFMOPR>2.0.CO;2.

[48] W. L. Weaver and R. N. Green, "Simulation study of geometric shape factor approach to estimating earth emitted flux densities from wide field-of-view radiation measurements," *Remote Sensing Environ*., vol. 9, pp. 265-276, 1980, DOI:10.1016/0034-4257(80)90033-4.

[49] G. L. Smith, R. N. Green, E. Raschke, L. M. Avis, J. T. Suttles, B. A. Wielicki, and R. Davies "Inversion methods for satellite studies of the Earth's Radiation Budget: Development of algorithms for the ERBE Mission," *Rev. Geophys*., vol. 24, no. 2, pp. 407–421, 1986, DOI:10.1029/RG024i002p00407.

[50] G. L. Smith and R. N. Green, "Deconvolution of wide field-of-view radiometer measurement of earth-emitted radiation. Part I: Theory," *J. Atmos. Sci*., vol. 38, pp. 461-473, 1981, DOI:10.1175/1520-0469(1981)038<0461:DOWFOV>2.0.CO;2.

[51] T. D. Bess, R. N. Green and G. L. Smith, "Deconvolution of wide field-of-view radiometer measurements of earth-emitted radiation. Part II: Analysis of first year of Nimbus 6 ERB wide angle earth-emitted data," *J. Atmos. Sci*., vol. 38, pp. 474-488, 1981, DOI:10.1175/1520-0469(1981)038<0474:DOWFOV>2.0.CO;2.

[52] R. N. Green, "The Effect of Data Analysis Techniques on the Interpretation of Wide-Angle Longwave Radiation Measurements," *J. Atmos. Sci*., vol. 38, pp. 2045–2055, 1981, DOI: 10.1175/1520-0469(1981)038<2045:TEODAT>2.0.CO;2.

[53] J. T. Suttles, R. N. Green, P. Minnis, G. L. Smith, W. F. Staylor, B. A. Wielicki, I. J. Walker, D. F. Young, V. R. Taylor, L. L. Stowe, "Angular radiation models for Earth-atmosphere system, 1, Shortwave radiation,", *NASA Ref. Publ., RP-1184-Vol 1*, 1988. [Online]. Available: https://hdl.handle.net/2060/19880018293.

[54] J. T. Suttles, R. N. Green, G. L. Smith, B. A. Wielicki, I. J. Walker, V. R. Taylor, L. L. Stowe, "Angular radiation models for the Earth-atmosphere system, 2, Longwave radiation," *NASA Ref. Publ., RP-1184-Vol 2*, 1989. [Online]. Available: https://hdl.handle.net/2060/19890011216.

[55] B. A. Wielicki, T. Wong, R. P. Allan, A. Slingo, J. T. Kiehl, B. J. Soden, C. T. Gordon, A. J. Miller, S.-K. Yang, D. A. Randall, F. Robertson, J. Susskind, and H. Jacobowitz, "Evidence for Large Decadal Variability in the Tropical Mean Radiative Energy Budget," *Science*, vol. 295, no. 5556, pp. 841-844, 2002, DOI:10.1126/science.1065837.

[56] S. Kato and N. G. Loeb, "Twilight Irradiance Reflected by the Earth Estimated from Clouds and the Earth's Radiant Energy System (CERES) Measurements," *J. Climate*, vol. 16, pp. 2646–2650, 2003, DOI:10.1175/1520-0442(2003)016<2646:TIRBTE>2.0.CO;2.

List of Table:

List of Figures:

with time. The dashed line (bottom plot) gives the best fit linear regression line to the daytime minus night-time longwave flux data (green line, bottom plot). Data Source [29].

Fig. 6. Time series of total channel offset (red squares, left axis) and shortwave channel offset (blue triangles, right axis) as determined from internal blackbody and night-side of the Earth, respectively, from 11/14/1984 to 9/30/1999. Note that the offsets themselves are much larger than the measured TOA signals, indicating the importance of accurate on-orbit internal calibrations and deep-space measurements. Data Source [35].

Fig. 7. The difference between ERBE nonscanner and ERBE scanner measurements for longwave (red) and shortwave (blue) flux for one ERBS satellite orbit. The x-axis is the satellite true anomaly in degree, which measures the satellite position relative to the Sun. Night time portion of the orbit is found approximately between 120º and 280º. Large changes in longwave flux differences occurred at the day-night boundary due to large changes in thermal loading conditions on the nonscanner instrument. Data Source [37].

Fig. 8. Changes in ERBS satellite altitude from 1985 to 1999 (top panel) and its effect (bottom panel) on the ERBS WFOV nonscanner longwave (red), shortwave (blue), and net (green) flux record over the 15-year period as seen in Edition2 (dash line with no altitude correction) and Edition3 data (solid line with altitude correction). ERBE/ERBS WFOV Edition3 data is a reprocess of the ERBE/ERBS WFOV Edition 2 data and incorporated satellite altitude correction to the data processing. Data Source [29].

Table:

TABLE I. Global annual mean ERBE Nonscanner TOA longwave (LW) and shortwave (SW) flux uncertainty (Wm^{-2}) after applying corrections.

Sources of uncertainty	LW	SW
Instrument stability[1]	±0.5	±0.1
Instrument absolute accuracy[2]	±2.5	±2.5
Intercalibration[3]	±1.2	±1.0
Nonscanner Inversion[4]	<±1.0	<±1.0
Satellite Altitude Correction[5]	0.0	0.0
Twilight data[6]	n/a	>0.2

1. Instrument stability uncertainty from gain variation at the end of 15-year period after 8.8% shortwave gain correction and 1.5% day/night longwave correction
2. Instrument absolute accuracy uncertainty due to offset variations after correcting for long-term offset drifts and instrument restart offset changes
3. Instrument intercalibration uncertainty reflecting uncertainty when calibrating ERBE nonscanner footprints with ERBE scanner observations
4. Inversion uncertainty for ERBE WFOV shape factor method
5. Uncertainty after applying 0.7% altitude correction over 15-year period
6. Longwave twilight uncertainty unavailable

Figures:

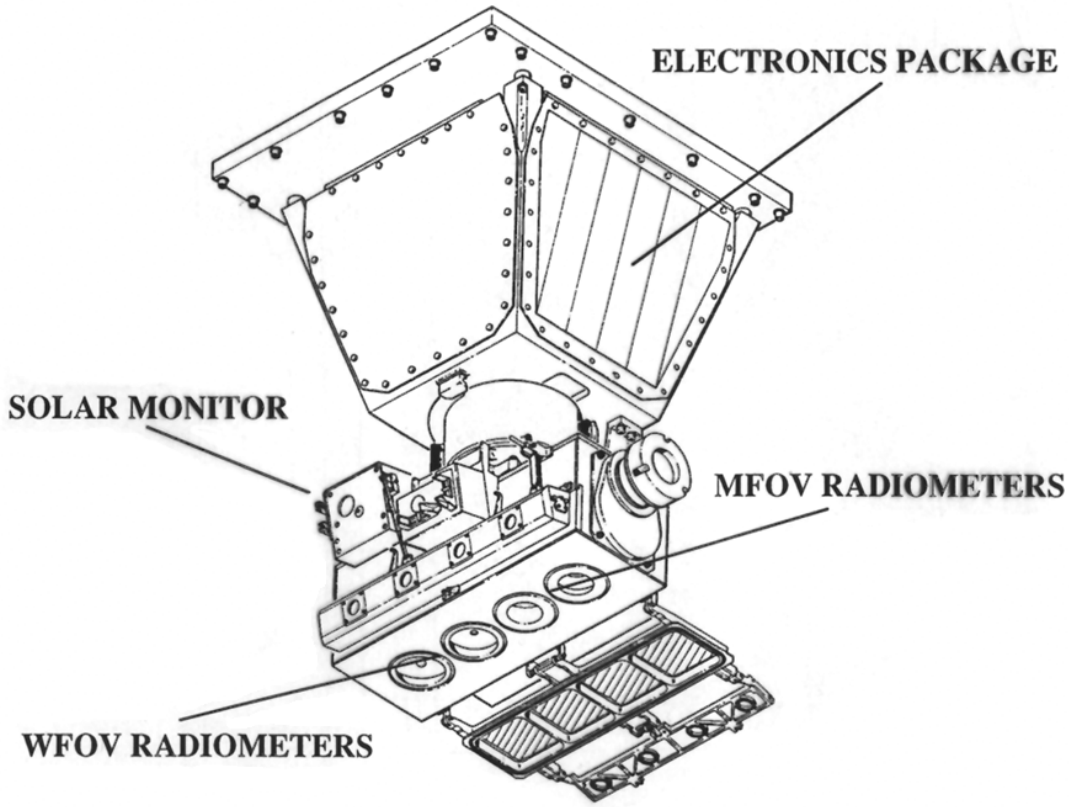

Fig. 1. ERBE nonscanner instrument package including the solar monitor, two MFOV radiometers located on the bottom right side of the picture and two WFOV radiometers located on the bottom left.

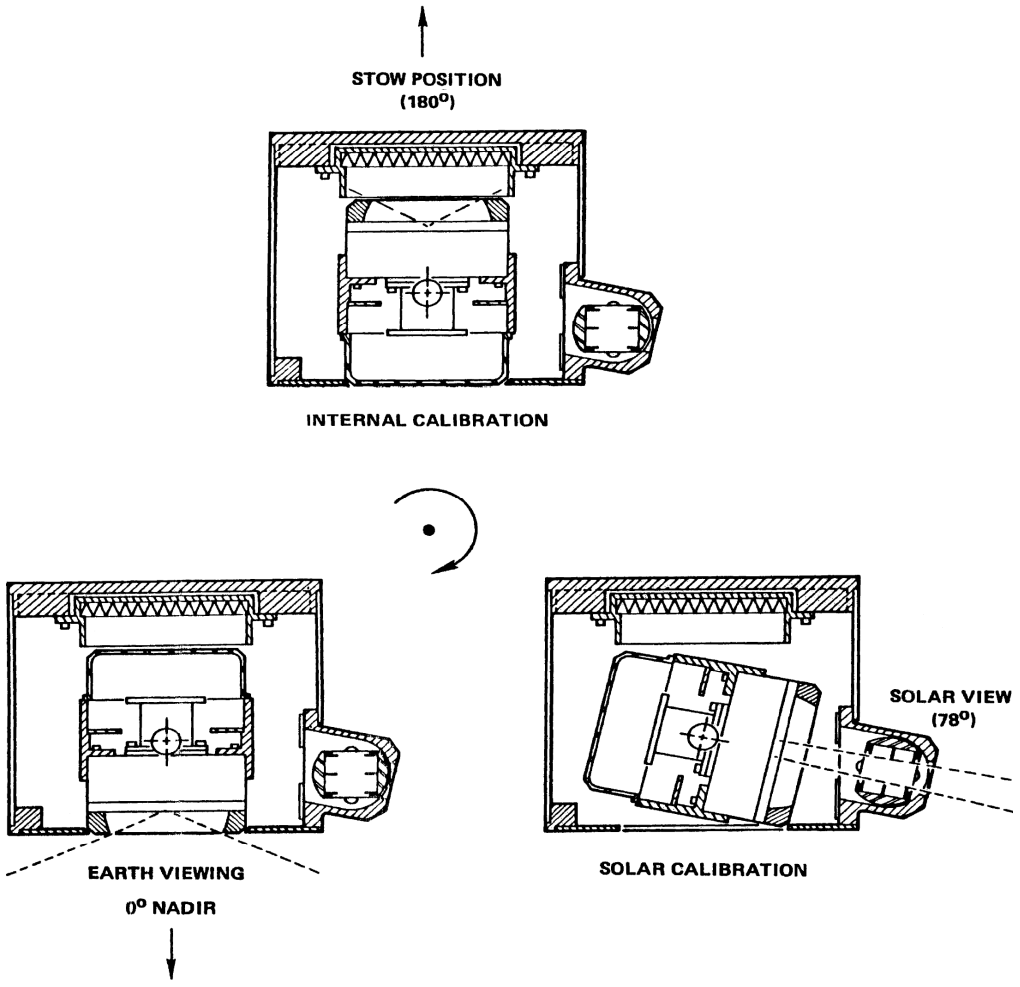

Fig. 2. ERBE nonscanner radiometer positions during bi-weekly on-orbit internal blackbody calibrations (stow position), bi-weekly on-orbit solar calibrations (solar view position), and normal nadir-pointing Earth-viewing observations.

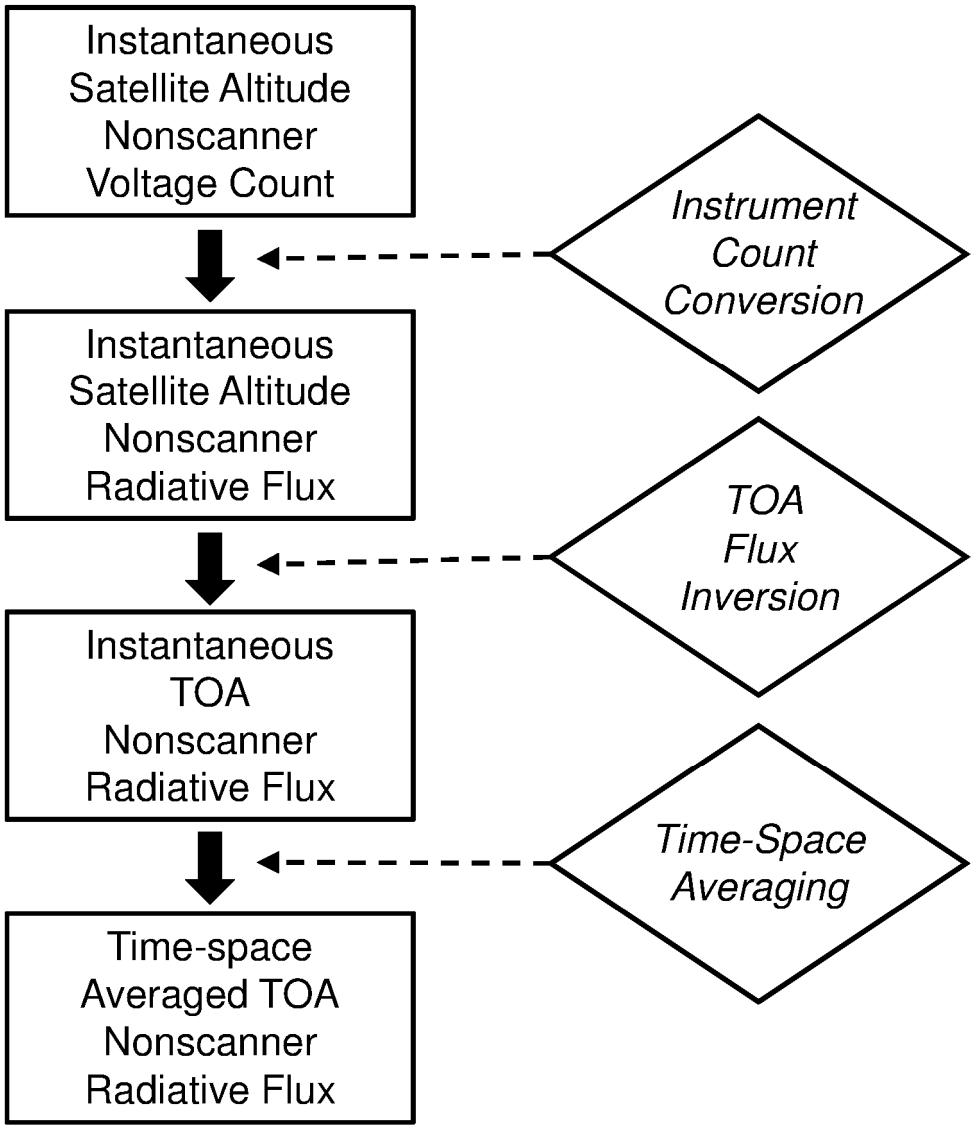

Fig. 3. ERBE nonscanner data processing system diagram.

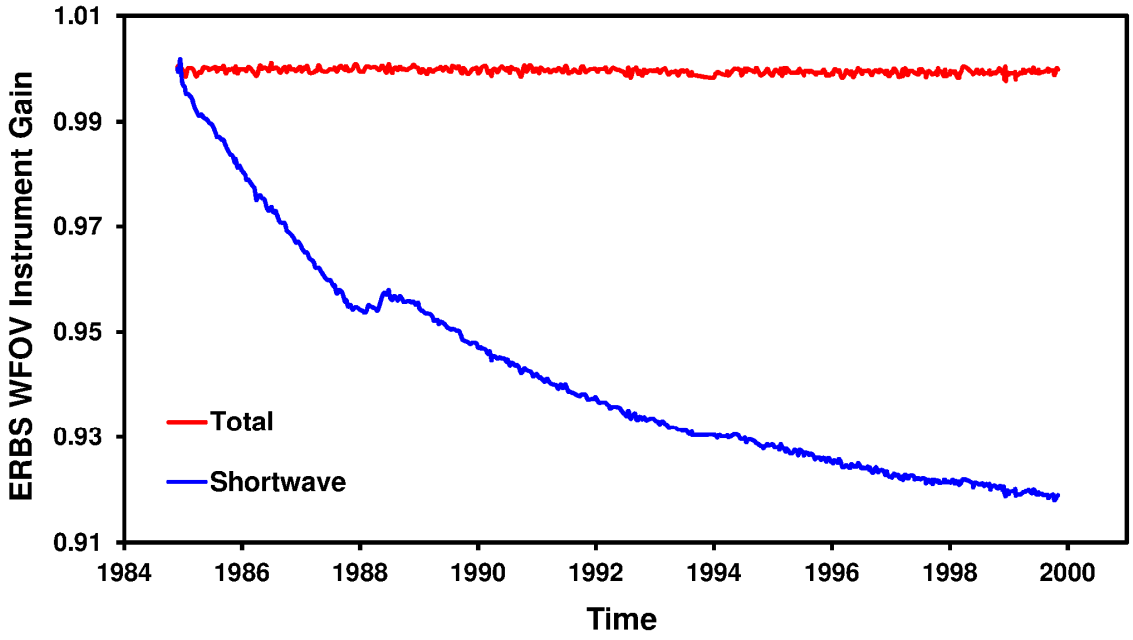

Fig. 4. Time history of the ERBS nonscanner instrument gain for the WFOV total radiometer (red) and the WFOV shortwave radiometer (blue) from 11/14/1984 to 9/30/1999. Note that the ERBS nonscanner shortwave gain increased slightly during 1988-89 period when atmospheric densities amplified at ERBS altitude associated with the maximum solar magnitude activity. The increased atomic oxygen concentrations from this event, acting as a bleaching agent, cleaned the shortwave filter dome surface slightly. Data Source [25].

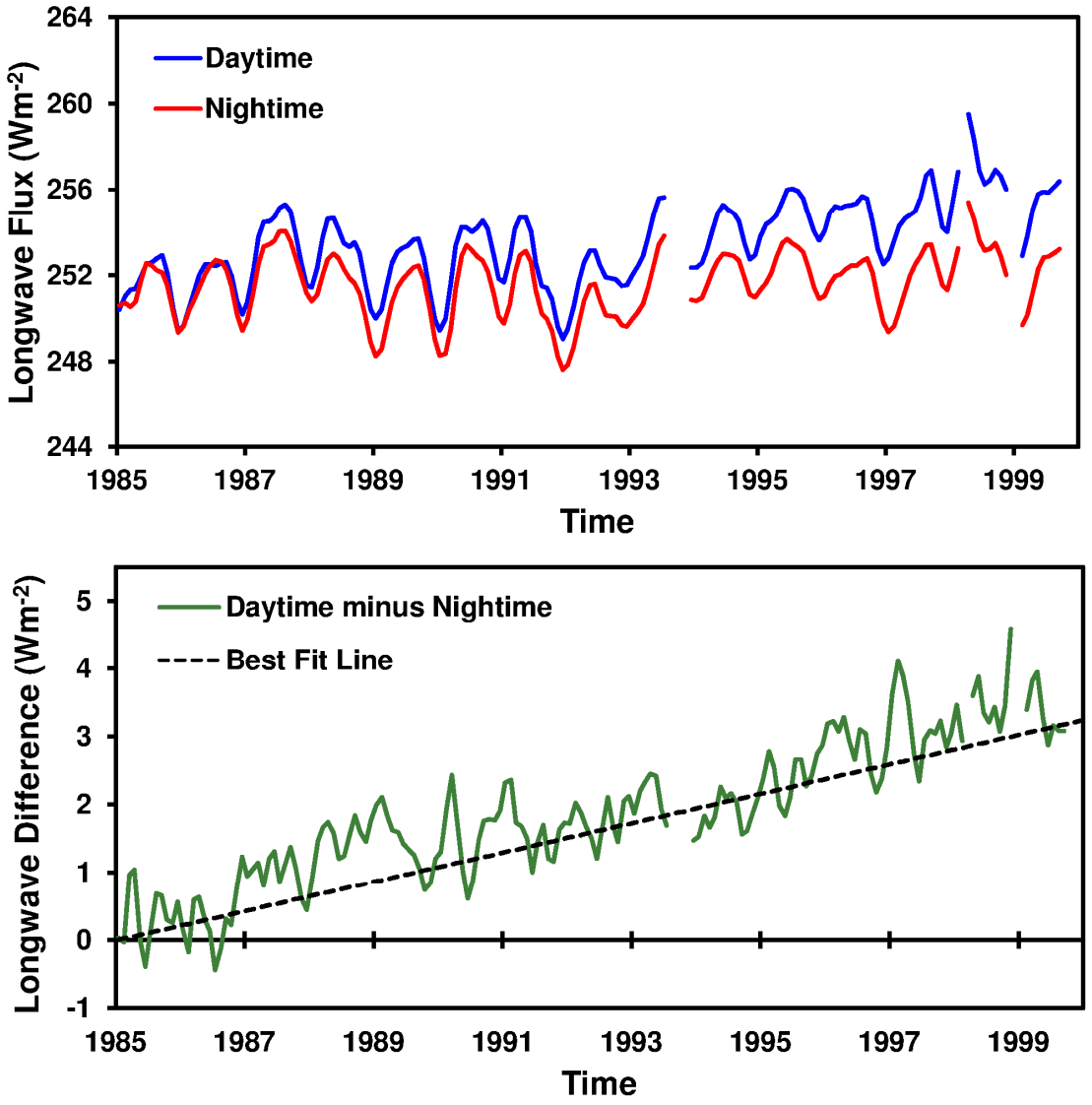

Fig. 5. Time history of the ERBS WFOV nonscanner daytime longwave flux (blue line, top plot) as determined by subtracting the shortwave channel from the total channel, which shows approximately constant nightime flux (red line, top plot). Daytime longwave flux would be expected to be similarly trend-free, yet it shows an increase with time. The dashed line (bottom plot) gives the best fit linear regression line to the daytime minus nightime longwave flux data (green line, bottom plot). Data Source [29].

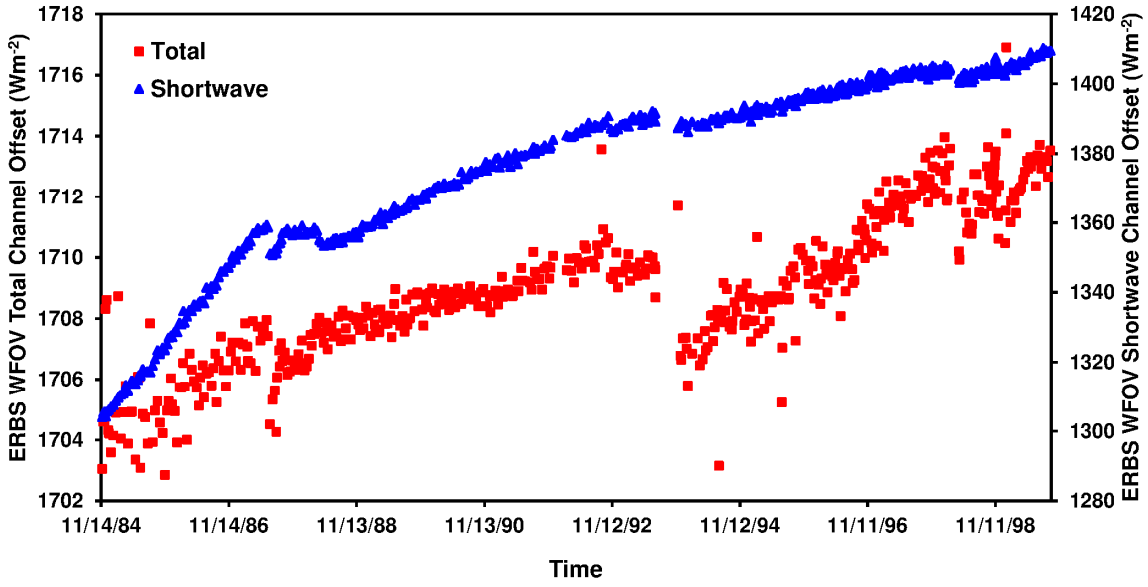

Fig. 6. Time series of total channel offset (red squares, left axis) and shortwave channel offset (blue triangles, right axis) as determined from internal blackbody and night-side of the Earth, respectively, from 11/14/1984 to 9/30/1999. Note that the offsets themselves are much larger than the measured TOA signals, indicating the importance of accurate on-orbit internal calibrations and deep-space measurements. Data Source [35].

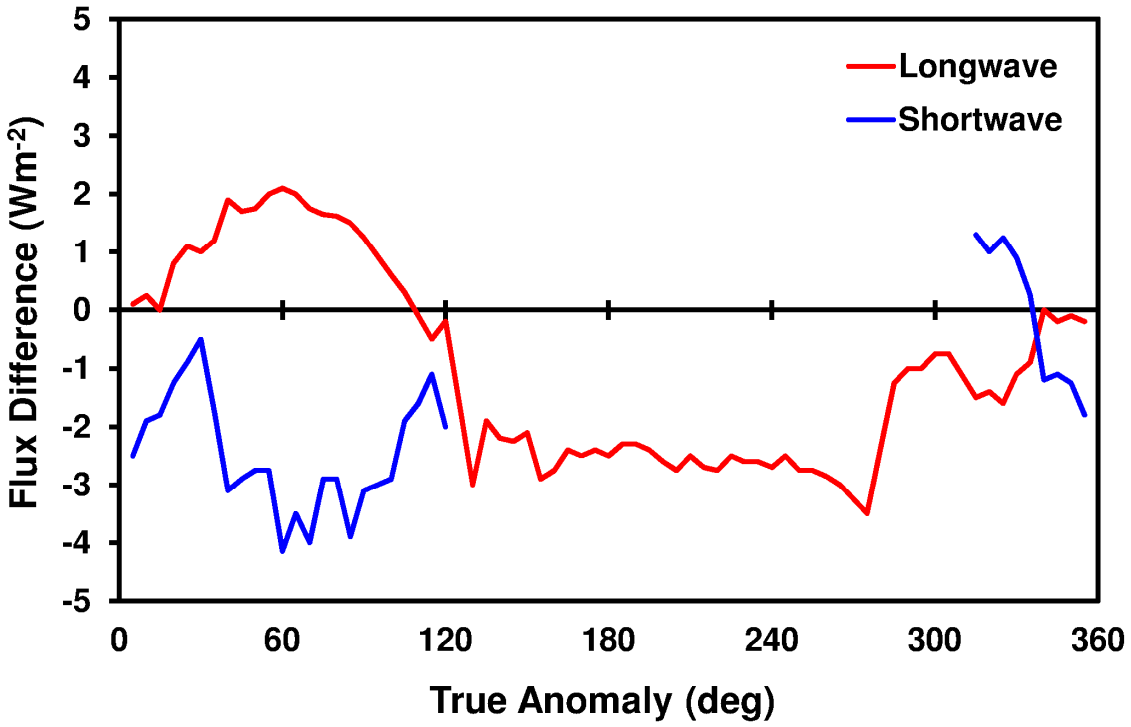

Fig. 7. The difference between ERBE nonscanner and ERBE scanner measurements for longwave (red) and shortwave (blue) flux for one ERBS satellite orbit. The x-axis is the satellite true anomaly in degree, which measures the satellite position relative to the Sun. Night time portion of the orbit is found approximately between 120º and 280º. Large changes in longwave flux differences occurred at the day-night boundary due to large changes in thermal loading conditions on the nonscanner instrument. Data Source [37].

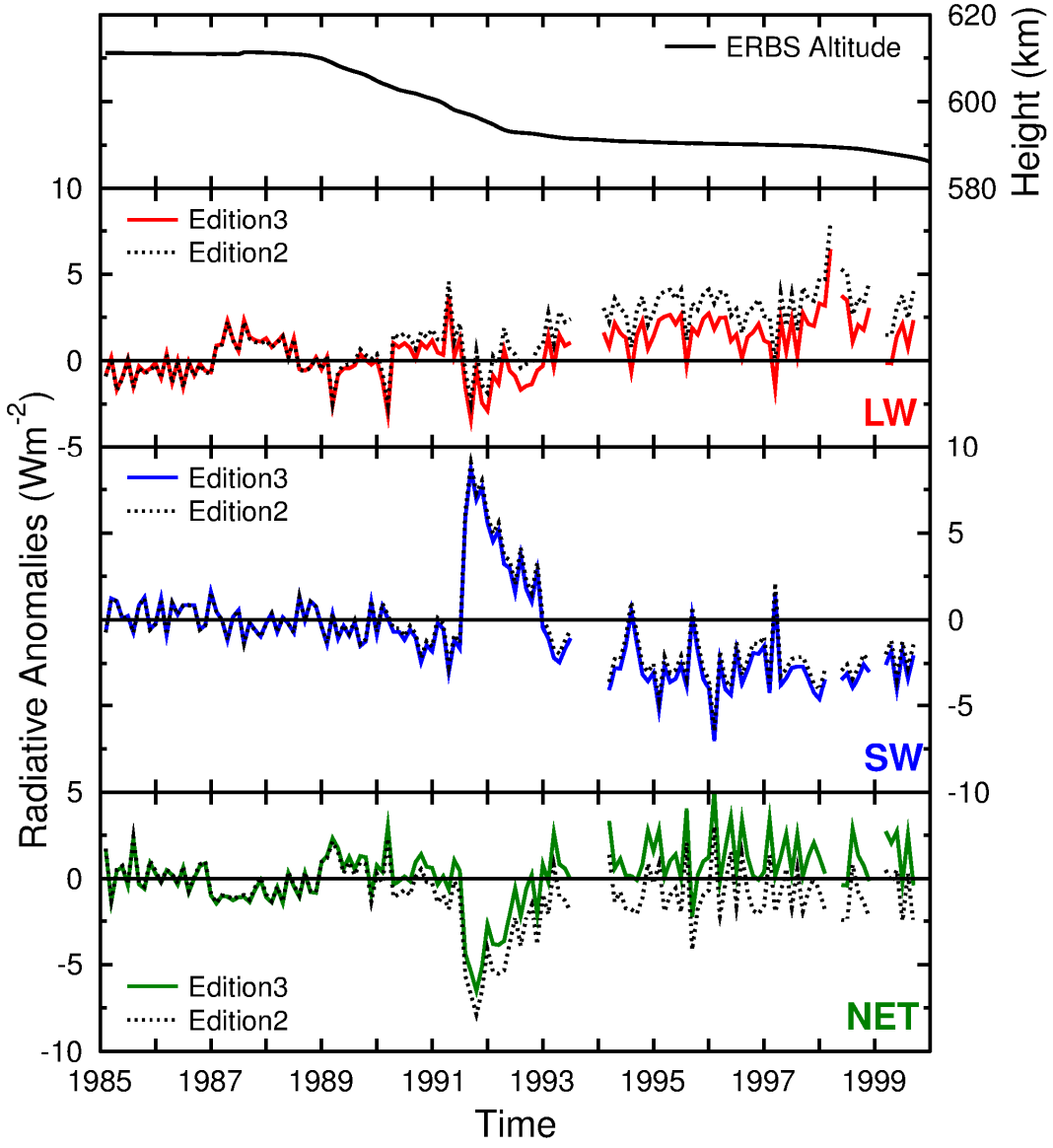

Fig. 8. Changes in ERBS satellite altitude from 1985 to 1999 (top panel) and its effect (bottom panel) on the ERBS WFOV nonscanner longwave (red), shortwave (blue), and net (green) flux record over the 15-year period as seen in Edition2 (dash line with no altitude correction) and Edition3 data (solid line with altitude correction). ERBE/ERBS WFOV Edition3 data is a reprocess of the ERBE/ERBS WFOV Edition2 data and incorporated satellite altitude correction to the data processing. Data Source [29].